

Laboratory modelling of the effects of temporal changes of estuarine-fresh-water discharge rates on the propagation speed of oceanographic coastal currents

PETER J. THOMAS¹† AND P. F. LINDEN²

¹Fluid Dynamics Research Centre, School of Engineering, University of Warwick,
Coventry CV4 7AL, UK

²Department of Applied Mathematics and Theoretical Physics, Centre for Mathematical Sciences,
Wilberforce Road, Cambridge CB3 0WA, UK

(Received 5 March 2010; revised 2 September 2010; accepted 8 September 2010)

In this paper, results of laboratory experiments simulating buoyancy-driven coastal currents produced by estuarine discharges into the ocean, are discussed. The responses of the propagation speeds of the currents to increases and decreases of the volumetric discharge rate at the source are investigated. For increasing discharge rate, we find that the mean speed of the current head displays a sharp rise some time after the source discharge condition has changed. In contrast, a decrease of the current speed following a decreasing discharge rate proceeds gradually. The current speed after acceleration or deceleration is found to be equal to the speed that would be expected had the discharge been at the higher or lower rate from the start of the experiment. The relative speed at which the information of the changed discharge condition at the source approaches the advancing current head from upstream, for both increasing and decreasing discharge rates, is found to be approximately one to three times the mean speed of the current. Further, we find that this transmission speed is 0.82 ± 0.20 times the propagation speed of a linear, long interfacial Kelvin wave.

Key words: geophysical and geological flows, gravity currents, rotating flows

1. Introduction

This paper describes laboratory simulations of oceanographic buoyancy-driven coastal currents. In the natural environment, such currents can develop when estuarine water is discharged into the ocean. The density of the estuarine water is lower than that of the more saline ocean water, causing it to float on and spread out over the surface of the sea. When the spreading exceeds the Rossby deformation scale, the dynamics of the discharge are affected by the Coriolis force arising from the rotation of the earth, and the estuarine water is confined to the coastal zone where it establishes a buoyancy-driven current flowing along the coast. One typical example of such coastal currents is the Columbia River Plume (Hickey *et al.* 1998); for further examples, refer to Thomas & Linden (2007) (hereinafter TL).

† Email address for correspondence: pjt1@eng.warwick.ac.uk

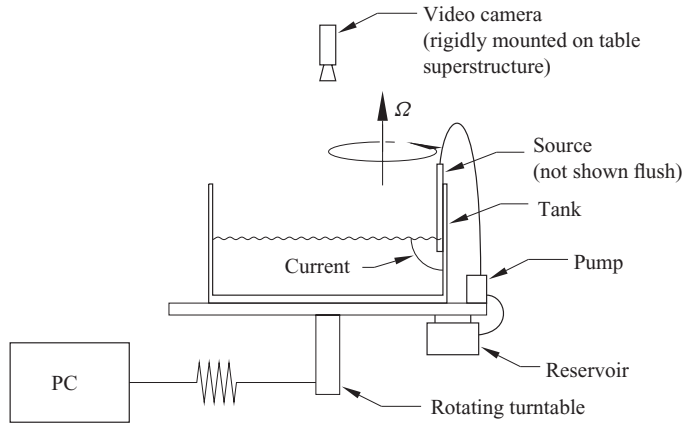


FIGURE 1. Sketch of the experimental set-up.

Previous studies of coastal currents (e.g. Griffiths & Hopfinger 1983, Griffiths 1986, Davies, Jacobs & Mofor 1993, Simpson 1997, Thomas & Linden 1998, Boyer, Haidvogel & Pèrenne 2001, Avicola & Huq 2002, Lentz & Helfrich 2002, Avicola & Huq 2003*a,b*, Rivas, Velasco Fuentes & Ochoa 2005, Horner-Devine *et al.* 2006 and TL) have dealt with the current speed, depth and width, and examined their stability and the effects of bottom topography on the current dynamics or the characteristics of the gyre that forms near the estuary where the river water enters the ocean. Here we examine the response of the propagation speed of the currents following a change of the volumetric discharge rate of fresh water at the source. In the natural environment, such a situation can arise, for instance, when the estuarine outflow suddenly increases after heavy inland rainfall or as a result of the diurnal and semi-diurnal tidal modulation of estuary discharge. We conduct laboratory experiments in which the source flow rate is changed instantaneously from one constant value to another, and measure the resulting change in the speed to the current. We also examine the time taken for the information about the change in flow rate to reach the front of the current and discuss the implications of the results obtained.

2. Experiments

The experiments were performed inside a transparent, circular acrylic tank, radius $R_S \approx 45$ cm, filled with salt water, density ρ_2 and centred on a turntable rotating about a vertical axis with constant angular velocity Ω . Estuarine discharges were simulated by releasing fresh water of density $\rho_1 < \rho_2$ from a small circular source mounted at the side wall of the tank. The fresh-water source was a vertical cylindrical tube with diameter 1 cm, and the outlet was adjusted to be level with the surface of the dense salt water inside the tank. Fresh water, dyed with food colouring for visualization, was supplied to the source by means of a calibrated peristaltic pump from a reservoir mounted on the turntable. The experiments were filmed from above with a video camera centred above the tank and co-rotating with the turntable (figure 1).

As in TL, the fresh water released at the source was discharged vertically upwards, rather than horizontally, as would be the case for estuarine discharges in the natural environment. The purpose of the vertical discharge direction was to minimize momentum flux effects and mixing of fresh water and salt water near the source.

The rotation rate of the tank was varied in the range $0.5 \text{ rad s}^{-1} \leq \Omega \leq 2.0 \text{ rad s}^{-1}$. The density difference between the fresh water and the salt water is characterized in

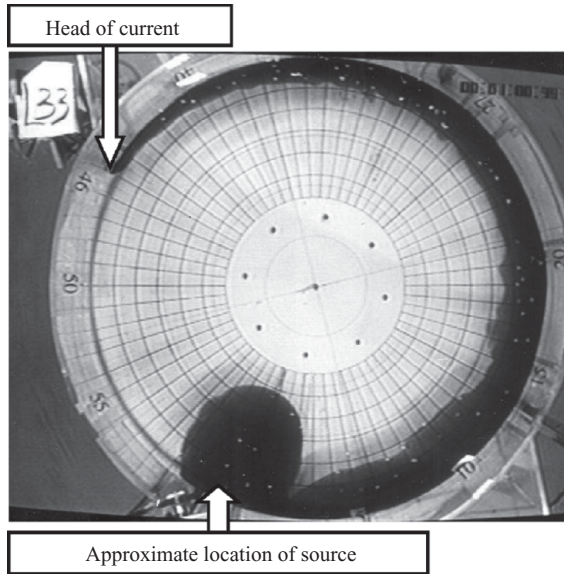


FIGURE 2. Flow visualizations showing a current (dark fluid) flowing along the wall of the circular tank. The turntable rotates anticlockwise ($\Omega > 0$). The current also propagates anticlockwise keeping the wall to its right.

terms of the reduced gravity defined as $g' \equiv g(\rho_2 - \rho_1)/\rho_1$, with $g = 981 \text{ cm s}^{-2}$. The reduced gravity was varied in the range $6.3 \text{ cm s}^{-2} \leq g' \leq 32.2 \text{ cm s}^{-2}$. The depth H of the salt water inside the tank was typically 10–15 cm. The currents occupied the upper 3–4 cm, and we observed no dependence of the current properties on H , suggesting that the lower layer is essentially passive in the parameter range of these experiments.

One main goal of the experiments was to investigate the speed by which the information that the volumetric discharge rate at the source has changed propagates along the length of the current. For this purpose, each experiment was started with a volumetric discharge rate q_0 at time $t = 0$. At a later time \hat{t} , when the front of the current was at a distance \hat{x} from the source, the flow rate was abruptly changed by an increment Δq . We conducted experiments in which the flow rate was increased from $q_0 = 6.4 \text{ cm}^3 \text{ s}^{-1}$ by three increments, $\Delta q = 5.6, 10.0, 19.7 \text{ cm}^3 \text{ s}^{-1}$. We also examined three cases where the initial flow rate was decreased from $q_0 = 26.1, 16.4, 12.0 \text{ cm}^3 \text{ s}^{-1}$ by three corresponding Δq -values down to the flow rate $q_1 = 6.4 \text{ cm}^3 \text{ s}^{-1}$.

We observed that the speed of the current, as measured by the rate of change of the position of the front with time, increased for increasing Δq while it decreased for decreasing Δq . We measured the time \tilde{t} , and the position \tilde{x} , of the current head at the onset of the acceleration or deceleration. The mean current speed at the instant, \tilde{t} , the current head changes speed is $u_m(\tilde{t}) = \tilde{x}/\tilde{t}$. The mean speed by which the information of the changed source condition travels along the current length is $u_w = u_w(\tilde{t}) = \tilde{x}/(\tilde{t} - \hat{t})$.

3. Experimental results

3.1. Qualitative observations

A photograph showing a typical current is shown in figure 2. The tank rotates counterclockwise, corresponding to the Northern hemisphere, and the current (dark

fluid) also propagates counterclockwise, keeping the wall of the tank to its right. A calibration grid was placed under the transparent bottom of the acrylic tank to aid with the data analysis. Each two successive concentric circles are spaced 5 cm apart while the angle of each sector is 0.1 rad. The approximate position of the fresh-water source is indicated in figure 2. Circumferential downstream positions along the wall of the tank are referred to by x and are relative to the source which is located at $x = 0$. The current length l is the circumferential distance between the source and the current head.

The current propagated around the circumference of the tank, and its width and depth decreased towards the front (figure 2). When the source flow rate was changed, there was no visible change to the appearance of the plan view of the current, neither near the source nor towards the front. The only detectable change was in the current speed at some time after the change in flow rate. The reason for the absence of a visible adjustment of the current width is probably related to the fact that the surface width seen in dye-visualization experiments is not the width relevant to the current dynamics (compare TL, pp. 54–59). Reference to figure 19 in TL reveals that the current width seen on the surface can be up to four times wider than w_0 . After increasing or decreasing the discharge rate at the source, there almost certainly exists a sub-surface width (and depth) adjustment to comply with the geostrophic scalings discussed in TL. However, the adjustment can be resolved only by illuminations of the current cross section, as illustrated in figure 17 of TL, but this was not possible during the present study.

Despite the lack of any visible evidence, based on analogous experiments on non-rotating gravity currents (Rottman & Simpson 1983), we expect that the source conditions are communicated by a wave or other nonlinear disturbance such as an internal bore. In our analysis of the quantitative data, we will explore this hypothesis, and discuss the propagation of source information in terms of a wave speed.

3.2. Typical raw data points

It is known (see e.g. Avicola & Huq 2002 and TL) that the propagation speeds of the currents and, hence their mean speeds u_m , decrease slightly during an experiment. Consequently, there exists the possibility that the information-propagation (wave) speeds u_w also change during an experiment. In order to resolve potential temporal changes of u_w , we conducted six identical runs for each set of experimental conditions of q_0 , Ω , g' and Δq , for six different times \hat{t} when the source flow rate was altered.

Figures 3 and 4 display typical measurements of the current length l as a function of time t . Figure 3 displays data for six experiments with identical values of q_0 , Ω and g' , for which the discharge rate was increased by a constant Δq at six different times, $\hat{t} \equiv t_{on}$. Figure 4 shows the data for the same values of Ω and g' , but with initially high q_0 , and where the discharge rate was decreased by the same Δq -value for six different times, $\hat{t} \equiv t_{off}$.

We conducted experiments for 11 sets of different combinations of Ω , g' and Δq . For each combination, we ran experiments for the cases of increasing and corresponding decreasing Δq , giving a total of 22 sets of experimental conditions. With six experiments for each parameter set, a total of 132 experimental runs were conducted.

Figure 3 reveals that the front speed increases abruptly some time after the source flow rate was increased. For instance, for the experiment in which the flow rate increased at $\hat{t} \equiv t_{on} = 26.45$ s (open squares), the current increased its speed at $t = \tilde{t} \approx 39$ s. Figure 4 reveals a corresponding deceleration of the current head in

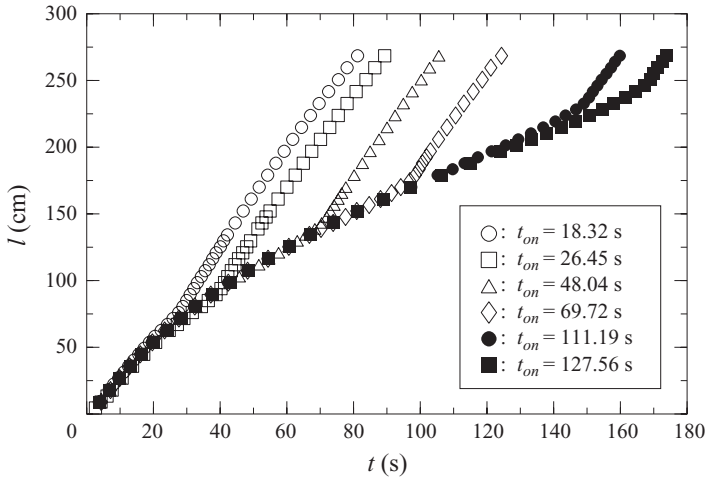


FIGURE 3. Current length l as a function of time t for six experiments with $\Omega = 2.0 \text{ rad s}^{-1}$ and $g' = 16.3 \text{ cm s}^{-2}$. In each experiment, flow rate at source increased by $\Delta q = 19.7 \text{ cm}^3 \text{ s}^{-1}$ from $q_0 = 6.4 \text{ cm}^3 \text{ s}^{-1}$ to $q_1 = 26.1 \text{ cm}^3 \text{ s}^{-1}$ at time $\hat{t} \equiv t_{on}$ identified in the key in the figure.

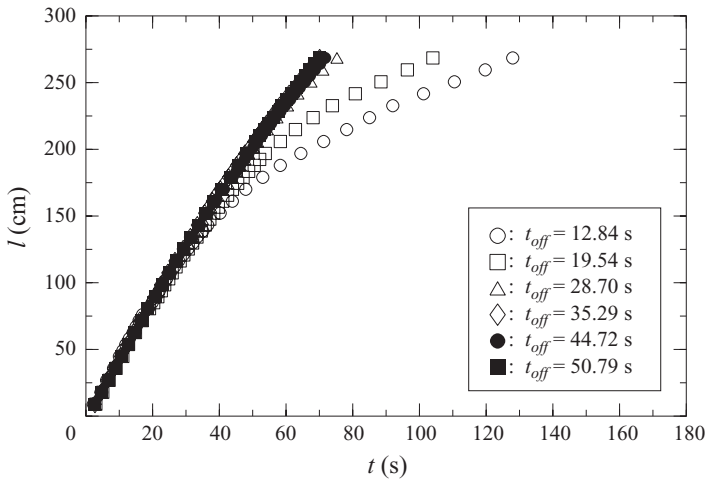


FIGURE 4. Current length l as a function of time t for six experiments with $\Omega = 2.0 \text{ rad s}^{-1}$ and $g' = 16.3 \text{ cm s}^{-2}$. In each experiment, flow rate at source decreased by $\Delta q = 19.7 \text{ cm}^3 \text{ s}^{-1}$ from $q_0 = 26.1 \text{ cm}^3 \text{ s}^{-1}$ to $q_1 = 6.4 \text{ cm}^3 \text{ s}^{-1}$ at time $\hat{t} \equiv t_{off}$ identified in the key in the figure.

experiments in which the flow rate was lowered. However, the onset of deceleration is substantially more gradual than the onset of acceleration.

Note that, during the data analysis, we used substantially magnified versions of the type of plots shown in figures 3 and 4. These displayed the individual data points as very small dots which substantially improves the resolution. For most experiments, it was then straightforward to interpolate the data manually and determine \tilde{t} . Here we had to use larger markers to identify data sets. As a consequence, it appears to be difficult to resolve \tilde{t} in figure 4, but this was not the case on the magnified plots. On these, the maximum error associated with determining \tilde{t} for experiments

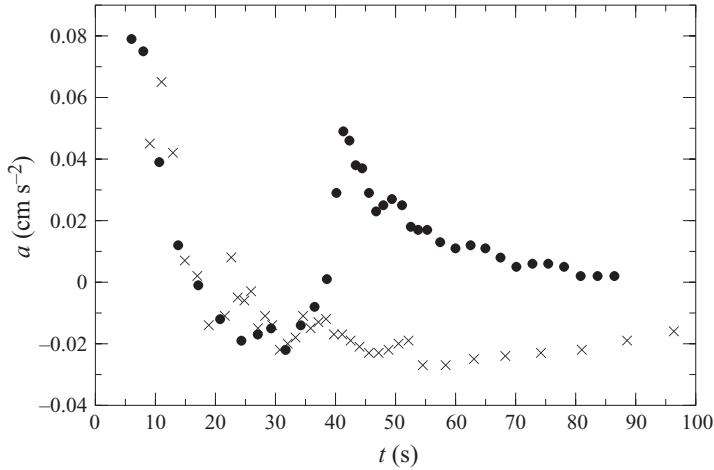


FIGURE 5. The current acceleration, a , as a function of the time, t , for the experiments with $t_{on} = 26.45$ s of figure 3 (●) and $t_{off} = 19.45$ s of figure 4 (×).

with increasing flow rates is approximately ± 1 s and ± 2 s for the experiments with decreasing flow rates.

3.3. The change of the mean speed of the currents

In order to determine the change in the mean speed of the current, we implemented the following procedure. At each time step t_i , when the current head is at location x_i , the mean speed of the current is given by $u_m(t_i) = x_i/t_i$. The change of the mean speed, $a_i = \Delta u_m(t_i)/\Delta t_i$, was determined by means of a central-difference-type scheme with $\Delta u_m(t_i) = u_b - u_a$, where $u_a = (x_{i+1} + x_i)/(t_{i+1} + t_i)$, $u_b = (x_{i+2} + x_{i+1})/(t_{i+2} + t_{i+1})$ and $\Delta t_i = t_b - t_a$, where $t_a = (1/2)(t_{i+1} + t_i)$, $t_b = (1/2)(t_{i+2} + t_{i+1})$.

Figure 5 displays the change of the acceleration a as a function of time for the data sets with $t_{on} = 26.45$ s and $t_{off} = 19.54$ s, shown in figures 3 and 4, respectively. Both currents initially accelerate from rest ($a > 0$) until $t \approx 17$ s when $a \approx 0$. The decrease of a with t is very similar for both currents despite their different values for q_0 . For $t > 17$ s, both currents begin to decelerate ($a < 0$). The current for which the flow rate at the source was increased (dots) undergoes a large positive acceleration at $t = \tilde{t} \approx 34 \pm 1$ s. The mean speed reaches a maximum around $t = 41$ s after which it again decreases gradually. The behaviour of the current for which the flow rate was reduced at $t_{off} = 19.45$ s (crosses) is different. Here the information that the flow rate had reduced reached the head of the current around $t = \tilde{t} \approx 26 \pm 2$ s. For $t > 26$ s, figure 5 reveals that the mean speed of the current simply continues to decrease gradually. In contrast to the behaviour of experiments with increased flow rates, there is no sudden sharp change of the mean speed.

A natural question to ask is whether, after the acceleration or deceleration resulting from the change in flow rate, the current adopts the speed associated with the new flow rate. Figures 6 and 7 show the current length as a function of time for, respectively, the cases of increased and decreased flow rate. The figures display dimensionless time $T = \Omega t$ and length $L = l/w_0$, where $w_0 = (g'q_0/\Omega^3)^{1/4}$ is the theoretical current width (see TL). After the onset of the acceleration/deceleration of the current, the data for $l(t)$ and t were re-scaled as $l' = l(t) - l(\tilde{t})$ and $t' = t - \tilde{t}$ before non-dimensionalization, to ensure that $l' = 0$ and $t' = 0$ when the current begins to accelerate/decelerate. For figure 6, the lower flow rate of $q_0 = 6.4 \text{ cm}^3 \text{ s}^{-1}$ was used to non-dimensionalize the data

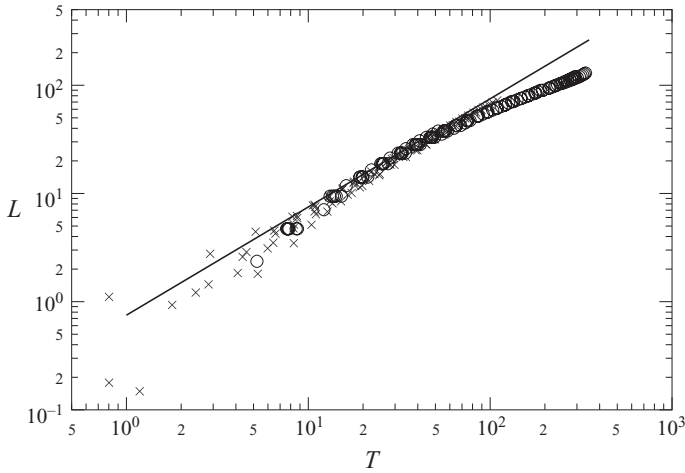


FIGURE 6. Non-dimensional current length L as a function of the non-dimensional time T . \circ before increase of flow rate; \times after increase of flow rate. The solid line represents the theoretical prediction, $L = (3/4)T$, of TL.

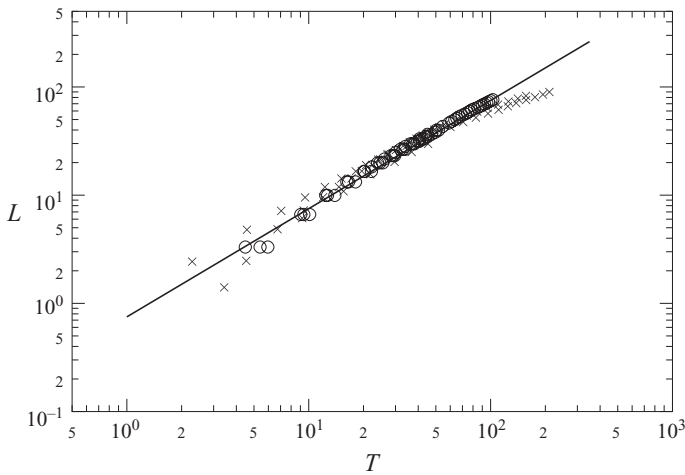


FIGURE 7. Non-dimensional current length L as a function of the non-dimensional time T . \circ before decrease of flow rate; \times after decrease of flow rate. The solid line represents the theoretical prediction, $L = (3/4)T$, of TL.

prior to the acceleration of the current head while the higher rate of $q_1 = 26.1 \text{ cm}^3 \text{ s}^{-1}$ was used for the data after the acceleration. Correspondingly, for figure 7, the higher flow rate of $q_0 = 26.1 \text{ cm}^3 \text{ s}^{-1}$ was used before the onset of deceleration while the lower rate of $q_1 = 6.4 \text{ cm}^3 \text{ s}^{-1}$ was used after deceleration has begun.

The solid lines shown in figures 6 and 7 represent the theoretical predictions $L = (3/4)T$ from the model of TL. The values of $L(T)$ from before (circles) and after (crosses) the acceleration/deceleration of the current collapse onto each other and agree with the theoretical line. This implies that the current speed after the flow rate has changed is equal to the speed it would have had if the volumetric discharge rate had been at the higher/lower rate from the start of the experiment.

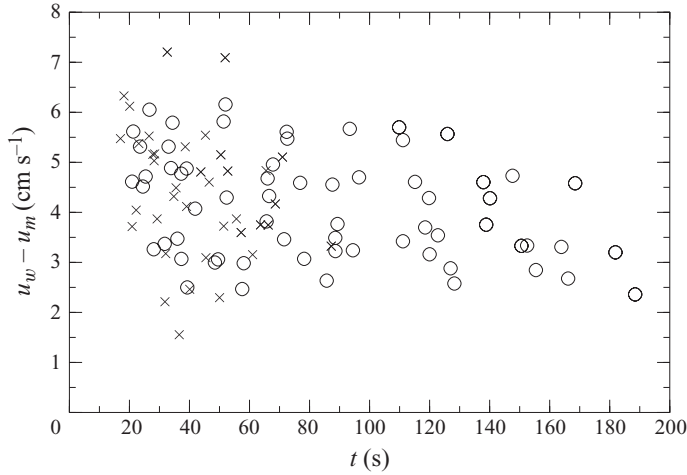


FIGURE 8. The relative wave speed, $u_w - u_m$, as a function of time, t . \circ increasing flow rate; \times decreasing flow rate at source.

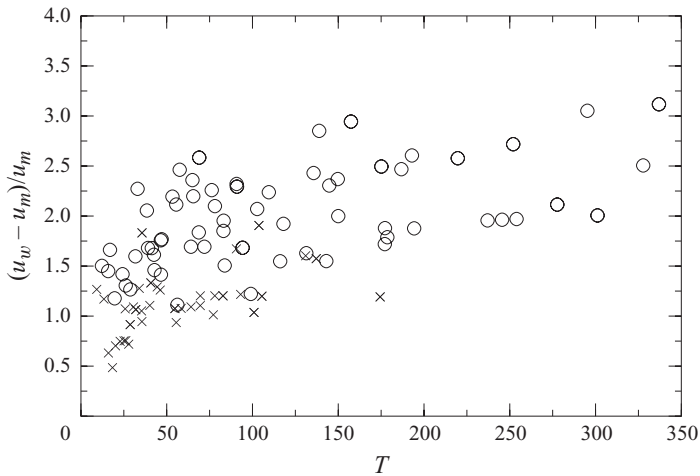


FIGURE 9. The ratio $(u_w - u_m)/u_m$ as a function of the non-dimensional time, T . \circ increasing flow rate; \times decreasing flow rate at source.

The good agreement of the experimental data in figures 6 and 7 with the predictions of the inviscid model of TL furthermore indicates that frictional effects on the currents are small. One reason for the increasing deviation from the model for larger times is the leakage of fluid from the main current near its surface (see TL, p. 61).

3.4. The speed of information transmission along the current

Figure 8 shows the relative speed, $u_w - u_m$, at which the information of the changed flow rate approaches the advancing current head from upstream for both increasing (circles) and decreasing (crosses) discharge rates. The values of $u_w - u_m$ are similar for increasing and decreasing flow rates and they possibly decrease slightly with time.

Figure 9 compares the relative speed with the mean speed of the current by displaying $(u_w - u_m)/u_m$ as a function of the non-dimensional time T . The data lie roughly within $1 \leq (u_w - u_m)/u_m \leq 3$, and the values increase with T . Moreover,

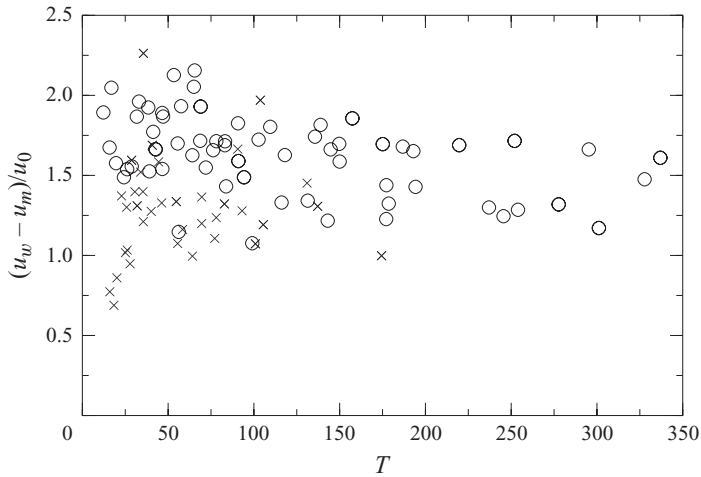


FIGURE 10. The ratio $(u_w - u_m)/u_0$ as a function of the non-dimensional time, T .
 ○ increasing flow rate; × decreasing flow rate at source.

the values for increasing flow rates (circles) are consistently higher than those for decreasing flow rates (crosses), showing that, compared to the mean speed of the current, the information that the discharge rate at the source has changed approaches the current head more slowly for reducing discharge rates than for rising discharge rates.

The geostrophic model in TL predicts a constant current propagation speed

$$u_0 = \frac{3}{4}(q_0 g' \Omega)^{1/4}. \tag{3.1}$$

Figure 10 compares the experimental data for the relative wave speed, $u_w - u_m$, of the present study to the value of u_0 given by (3.1), as a function of the dimensionless time T . The values of u_0 are calculated using the initial value q_0 . The relative wave speed lies roughly within the range $1 \leq (u_w - u_m)/u_0 \leq 2$. Averaging the values of all data yields a mean value of $(u_w - u_m)/u_0 = 1.54 \pm 0.37$. The mean value obtained for increasing flow rates (circles) is 1.62 ± 0.24 while value for decreasing flow rates (crosses) is 1.40 ± 0.50 .

One candidate for the transmission of information along the current is an interfacial Kelvin wave. The propagation speed of a long, linear Kelvin wave is $u_K = \sqrt{g'h}$. Using the current depth $h_0 = \sqrt{4\Omega q_0/g'}$ (see, e.g. TL) for h in the expression for the speed of the Kelvin wave yields

$$u_K = \sqrt{2}(q_0 g' \Omega)^{1/4}. \tag{3.2}$$

Comparison of (3.2) with (3.1) reveals that both differ only by the numerical value of the factor on the right-hand side of the equations. Consequently, we can infer the ratio $(u_w - u_m)/u_K$ from the data shown in figure 10 through multiplication by $(3/4)/\sqrt{2} \approx 0.53$. This conversion gives $(u_w - u_m)/u_K = 0.82 \pm 0.20$, averaged over all the data, 0.86 ± 0.13 for increasing flow rates and 0.74 ± 0.27 for decreasing flow rates. Since these values are comparable with, but less than, the long Kelvin wave speed, our results support an interfacial Kelvin wave as one possible transmission mechanism for the information about the changed flow rate at the source.

4. Summary and conclusions

We have presented measurements of the average speed of buoyancy-driven coastal currents produced in the laboratory by a source of buoyant fluid adjacent to a vertical boundary in a rotating fluid. We observed that the mean speeds of the currents undergoes a sudden, sharp rise some time after the volumetric fresh-water discharge rate at the source has increased. In contrast, when the discharge rate at the source is decreased, there exists no corresponding sharp drop of the mean speed when the information of the changed discharged condition reaches the current head. For decreasing volumetric flow rates at the source, the decrease of the mean current speed that follows occurs gradually. We found that the speed a current eventually adopts after an increase or decrease in flow rate is equal to the speed that corresponds to the new flow rate.

From measurements of the time taken for the current to accelerate or decelerate after the flow rate is altered, we inferred that the transmission of information along the current travels one to three times faster than the current itself. A comparison with the speed of a linear interfacial Kelvin wave showed that this transmission speed is 0.82 ± 0.20 of the long-wave speed. This relationship, which holds for all the experimental parameters, suggests that the Kelvin wave, which, like the current itself, propagates cyclonically, provides a possible mode for the information transmission. However, since the Kelvin wave speed is simply a speed given by a combination of the relevant parameters, it is possible that the actual mode could be some other form such as a gravity current or internal bore. In some experiments, particles placed on the surface at the time the flow rate is increased were observed to travel along the current at the speed of the disturbance, suggesting that nonlinear advection in the form of a gravity current may be responsible for the transmission of source information. This would explain the different acceleration behaviour of the current head following increases and decreases of the discharge rate at the source. While the present results probably favour a gravity current as the transmission mechanism, only in-depth particle-image-velocimetry (PIV) data could resolve the issue.

For the Columbia River Plume, Hickey *et al.* (1998) report that the flow into the estuary varies between $3000 \text{ m}^3 \text{ s}^{-1} \leq q_0 \leq 17000 \text{ m}^3 \text{ s}^{-1}$ over a typical year. The salinity of ocean water quoted is 32 psu, corresponding to $g' \approx 0.2 \text{ m s}^{-2}$. Using the vertical component of the rotation rate of the earth at latitude (46° N), $\Omega = 5.2 \times 10^{-5} \text{ rad s}^{-1}$, the propagation speed of the Kelvin wave follows from (3.2) as $0.60 \text{ m s}^{-1} \leq u_K \leq 0.92 \text{ m s}^{-1}$. This implies that within a typical tidal period, Δt_{tp} , of six hours, the Kelvin wave can travel a distance $x_K = u_K \Delta t_{tp}$ in the range $13 \text{ km} \leq x_K \leq 20 \text{ km}$. The associated Rossby deformation scale, $R_D = \sqrt{g'h_0}/\Omega = u_K/\Omega$, for the discharges of the Columbia River Plume has values within $12 \text{ km} \leq R_D \leq 18 \text{ km}$, which is of the same order of magnitude as x_K . Hence, it can be concluded that, within a tidal period, the information of a changed discharge rate at the source can travel a distance relative to the advancing current, which is equal to approximately one Rossby deformation scale.

REFERENCES

- AVICOLA, G. & HUQ, P. 2002 Scaling analysis for the interaction between a buoyant coastal current and the continental shelf: experiments and observations. *J. Phys. Oceanogr.* **32**, 3233–3248.
- AVICOLA, G. & HUQ, P. 2003a The role of the outflow geometry in the formation of the recirculating bulge region in coastal buoyant outflows. *J. Marine Res.* **61**, 411–434.

- AVICOLA, G. & HUQ, P. 2003b The characteristics of the recirculating bulge region in coastal buoyant outflows. *J. Marine Res.* **61**, 435–463.
- BOYER, D. L., HAIDVOGEL, D. B. & PÉRENNE, N. 2001 Laboratory–numerical comparisons of flow over a coastal canyon. *J. Atmos. Tech.* **18**, 1698–1718.
- DAVIES, P. A., JACOBS, P. T. G. A. & MOFOR, L. A. 1993 A laboratory study of buoyant fresh water boundary currents in tidal crossflows. *Oceanol. Acta* **16**, 489–503.
- GRIFFITHS, R. W. 1986 Gravity currents in rotating systems. *Annu. Rev. Fluid Mech.* **18**, 59–89.
- GRIFFITHS, R. W. & HOPFINGER, E. J. 1983 Gravity currents moving along a lateral boundary in a rotating fluid. *J. Fluid Mech.* **134**, 357–399.
- HICKEY, B. M., PIETRAFESA, L. J., JAY, D. A. & BOICOURT, W. C. 1998 The Columbia River Plume Study: subtidal variability in the velocity and salinity fields. *J. Geophys. Res.* **103** (C5), 10339–10368.
- HORNER-DEVINE, A. R., FONG, D. A., MONISMITH, S. G. & MAXWORTHY, T. 2006 Laboratory experiments simulating coastal river inflow. *J. Fluid Mech.* **555**, 203–232.
- LENTZ, S. J. & HELFRICH, K. R. 2002 Buoyant gravity currents along a sloping bottom in a rotating fluid. *J. Fluid Mech.* **464**, 251–278.
- RIVAS, D., VELASCO FUENTES, O. U. & OCHOA, J. 2005 Topographic effects on the dynamics of gravity currents in a rotating system. *Dyn. Atmos. Oceans* **39**, 227–249.
- ROTTMAN, J. W. & SIMPSON, J. E. 1983 Gravity currents produced by instantaneous releases of a heavy fluid in a rectangular channel. *J. Fluid Mech.* **135**, 95–110.
- SIMPSON, J. E. 1997 *Gravity Currents in the Environment and the Laboratory*, 2nd edn. Cambridge University Press.
- THOMAS, P. J. & LINDEN, P. F. 1998 A bi-modal structure imposed on gravity-driven boundary currents in rotating systems by effects of the bottom topography. *Exp. Fluids* **25**, 388–391.
- THOMAS, P. J. & LINDEN, P. F. 2007 Rotating gravity currents: small-scale and large-scale laboratory experiments and a geostrophic model. *J. Fluid Mech.* **578**, 35–65.